NANO LETTERS

Letter

pubs.acs.org/NanoLett

Near Full-Composition-Range High-Quality $GaAs_{1-x}Sb_x$ Nanowires Grown by Molecular-Beam Epitaxy

Lixia Li,[†] Dong Pan,*[,†] Yongzhou Xue,[†] Xiaolei Wang,[†] Miaoling Lin,[†] Dan Su,[†] Qinglin Zhang,[‡] Xuezhe Yu,[†] Hyok So,[†] Dahai Wei,[†] Baoquan Sun,[†] Pingheng Tan,[†] Anlian Pan,*[,‡] and Jianhua Zhao*[,†]

[†]State Key Laboratory of Superlattices and Microstructures, Institute of Semiconductors, Chinese Academy of Sciences, P.O. Box 912, Beijing 100083, China

[‡]Key Laboratory for Micro-Nano Physics and Technology of Hunan Province, School of Physics and Microelectronic Science, and State Key Laboratory of Chemo/Biosensing and Chemometrics, Hunan University, Changsha 410082, China

S *Supporting Information*

ABSTRACT: Here we report on the Ga self-catalyzed growth of near full-composition-range energy-gap-tunable $GaAs_{1-x}Sb_x$ nanowires by molecular-beam epitaxy. $GaAs_{1-x}Sb_x$ nanowires with different Sb content are systematically grown by tuning the Sb and As fluxes, and the As background. We find that $GaAs_{1-x}Sb_x$ nanowires with low Sb content can be grown directly on Si(111) substrates ($0 \le x \le 0.60$) and GaAs nanowire stems ($0 \le x \le 0.50$) by tuning the Sb and As fluxes. To obtain $GaAs_{1-x}Sb_x$ nanowires with x ranging from 0.60 to 0.93, we grow the $GaAs_{1-x}Sb_x$ nanowires on GaAs nanowire stems by tuning the As background. Photoluminescence measurements confirm that the emission wavelength of the $GaAs_{1-x}Sb_x$ nanowires is tunable from 844 nm (GaAs) to 1760 nm ($GaAs_{0.07}Sb_{0.93}$). High-resolution transmission electron microscopy images show that the grown $GaAs_{1-x}Sb_x$ nanowires have pure zinc-blende crystal structure. Room-temperature Raman spectra reveal a redshift of the optical phonons in the $GaAs_{1-x}Sb_x$ nanowires with x increasing from 0 to 0.93. Field-effect transistors based on individual $GaAs_{1-x}Sb_x$ nanowires are fabricated, and rectifying behavior is observed in devices with low Sb content, which disappears in devices with high Sb content. The successful growth of high-quality $GaAs_{1-x}Sb_x$ nanowires with near full-range bandgap tuning may speed up the development of high-performance nanowire devices based on such ternaries.

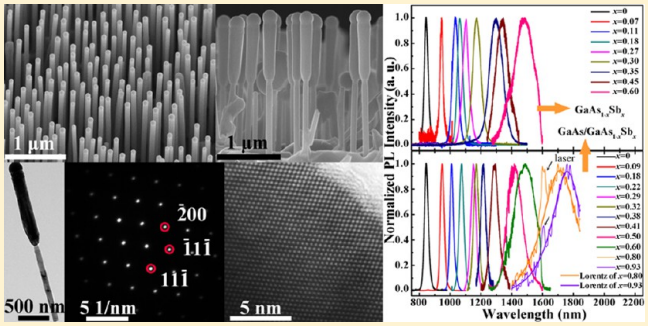

KEYWORDS: *$GaAs_{1-x}Sb_x$, nanowires, bandgap tuning, self-catalyzed, molecular-beam epitaxy, rectifying behavior*

As one of the most important narrow-bandgap ternary alloy semiconductors, $GaAs_{1-x}Sb_x$ has a bandgap tunable over a large range from about 870 nm (GaAs) to 1720 nm (GaSb) at room temperature, which makes it an attractive material for band structure engineering[1−3] and various optoelectronic applications, such as in optical fiber communication systems,[4] infrared light-emitting diodes,[5] photodetectors,[7] lasers,[1,6,8] and heterojunction bipolar transistors.[9] In addition, the $GaAs_{1-x}Sb_x$ semiconductor alloy is also a good candidate for study on spintronic devices based on GaAs.[10−12] However, the fabrication of high-quality and high Sb content $GaAs_{1-x}Sb_x$ films remains a challenge because there is a large lattice mismatch between the $GaAs_{1-x}Sb_x$ films and III−V semiconductor substrates, and the crystalline quality of the films is very sensitive to growth conditions.[9,13,14]

Because of the ability to relax the elastic strain in two dimensions,[15,16] III−V semiconductor nanowires provide a pathway to obtain high-quality antimony-based ternary materials. The quasi-one-dimensional geometry facilitates coherent growth of these ternary nanowires such as GaAsP, InAsSb, InPSb, and GaInSb[17−23] as well as the formation of strained, dislocation-free heterostructures in lattice mismatched systems.[24,25] Among them, $GaAs_{1-x}Sb_x$ nanowires are particularly interesting; several reports have been published on the growth of $GaAs_{1-x}Sb_x$ nanowires employing different growth techniques. Using metal−organic chemical vapor deposition (MOCVD) and metal−organic vapor phase epitaxy (MOVPE), gold-seeded $GaAs_{1-x}Sb_x$ ($0.09 \le x \le 0.60$) nanowires have been grown on GaAs nanowire stems;[26,27] gold-catalyzed pure GaSb nanowires have also been grown on GaAs and InAs nanowire stems, respectively.[24,28−35] $GaAs_{1-x}Sb_x$ and pure GaSb nanowires were also grown on Si substrates using gold catalysts by chemical vapor deposition.[36,37] Recently, much attention has been paid to molecular-beam epitaxy (MBE) growth of $GaAs_{1-x}Sb_x$ nanowires. By MBE, gold-free $GaAs_{1-x}Sb_x$ ($0 \le x \le 0.44$) nanowires have been grown on Si(111) substrates;[38−41] gold and gold-free $GaAs_{1-x}Sb_x$ ($x \le 0.43$) nanowire inserts have been grown on GaAs nanowire stems.[42−47] However, the focuses of the majority of current

Received: August 8, 2016
Revised: December 17, 2016
Published: January 19, 2017

DOI: 10.1021/acs.nanolett.6b03326
Nano Lett. 2017, 17, 622−630

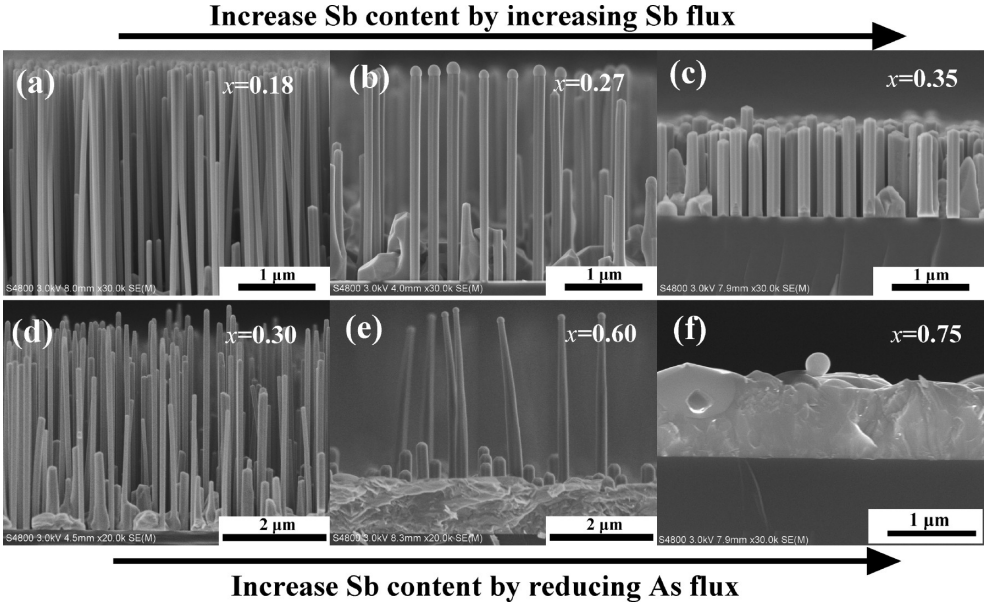

Figure 1. Side-view SEM images of the Ga self-catalyzed $GaAs_{1-x}Sb_x$ nanowires grown on Si(111) substrates by MBE. (a–c) $GaAs_{1-x}Sb_x$ nanowires were obtained by increasing Sb flux and corresponding x are 0.18, 0.27, and 0.35, respectively. (d–f) $GaAs_{1-x}Sb_x$ nanowires were obtained by reducing As flux and corresponding x are 0.30, 0.60, and 0.75, respectively.

MBE work have been on crystal structure,[39,41−44,46,47] electronic[40] and optical properties[38,40,41,45,48] of $GaAs_{1-x}Sb_x$ nanowires and nearly all the investigated nanowires have x lower than 0.50. Until now, to the best of our knowledge, the systematic growth and investigation of large-range wavelength-tunable high-quality $GaAs_{1-x}Sb_x$ nanowires by MBE have not yet been reported.

In this work, we report the growth of near full-composition-range $GaAs_{1-x}Sb_x$ nanowires by MBE. $GaAs_{1-x}Sb_x$ nanowires with different Sb content are systematically grown by tuning the Sb and As fluxes and the As background. We find that $GaAs_{1-x}Sb_x$ nanowires with low Sb content can be grown directly on Si(111) substrates ($0 \le x \le 0.60$) and GaAs nanowire stems ($0 \le x \le 0.50$) by tuning the Sb and As fluxes. To obtain $GaAs_{1-x}Sb_x$ nanowires with x ranging from 0.60 to 0.93, we grow the $GaAs_{1-x}Sb_x$ nanowires on GaAs nanowire stems by tuning the As background. To the best of our knowledge, it is the broadest Sb composition range in $GaAs_{1-x}Sb_x$ nanowires grown by MBE. Photoluminescence (PL) results confirm that the emission wavelength of the $GaAs_{1-x}Sb_x$ nanowires can be tuned from 844 nm (GaAs) to 1760 nm ($GaAs_{0.07}Sb_{0.93}$). The $GaAs_{1-x}Sb_x$ nanowires have pure zinc-blende (ZB) crystal structure. Optical phonons of the $GaAs_{1-x}Sb_x$ nanowires show redshift with x increasing from 0 to 0.93. Field-effect transistors (FETs) based on individual $GaAs_{1-x}Sb_x$ nanowires have been fabricated and rectifying behavior is observed in devices with low Sb content, which disappears in devices with high Sb content. The broad tunability of this antimony-based ternary alloy opens up new band-engineering opportunities for next-generation near-IR light emitting diodes, lasers, optical fiber communication, and so forth.

Experimental Details. All $GaAs_{1-x}Sb_x$ nanowires were grown in a solid source MBE system (VG 80). Commercial p-type Si(111) wafers were used as the substrates. Before being loaded into the MBE chamber, the Si substrates were pretreated by chemical etching using the method reported in our previous work.[49] For the growth of $GaAs_{1-x}Sb_x$ nanowires with low Sb content, $GaAs_{1-x}Sb_x$ nanowires were grown directly on Si substrates and GaAs nanowire stems, respectively, and the variation of Sb content was realized both by tuning the Sb and As fluxes. For the former, the Sb and As fluxes were ranged from 4.50×10^{-7} to 1.43×10^{-6} Torr and 4.20×10^{-7} to 1.61×10^{-6} Torr, respectively. For the later, the Sb and As fluxes were ranged from 3.75×10^{-7} to 1.83×10^{-6} Torr and 9.75×10^{-7} to 1.61×10^{-6} Torr, respectively. To obtain $GaAs_{1-x}Sb_x$ nanowires with higher Sb content, we grew the $GaAs_{1-x}Sb_x$ nanowires on GaAs nanowire stems by tuning the As background. The As background flux was ranged from 9.75×10^{-7} to 5.90×10^{-6} Torr. All the detailed growth procedures, growth parameters, and equipments for $GaAs_{1-x}Sb_x$ nanowire growth and characterization are given in Supporting Information Section 1.

$GaAs_{1-x}Sb_x$ Nanowires Growth on Si(111) Substrates by Tuning the Sb and As Fluxes. We began our work by growing $GaAs_{1-x}Sb_x$ nanowires directly on Si(111) substrates and Sb content of the nanowires was varied by tuning the Sb and As fluxes. Figure 1a–c shows the side-view scanning electron microscopy (SEM) images of the $GaAs_{1-x}Sb_x$ nanowires grown with Sb flux of 4.50×10^{-7}, 6.75×10^{-7}, and 1.43×10^{-6} Torr, respectively. It is evident from Figure 1 that $GaAs_{1-x}Sb_x$ nanowires have been successfully grown on the Si substrate surface, and all of them grow along the [111] direction (a typical 25° tilted SEM image is shown in Supporting Information Figure S1). Notably, the morphologies of $GaAs_{1-x}Sb_x$ nanowires are affected by the Sb flux. On one hand, the $GaAs_{1-x}Sb_x$ nanowire diameter increases with higher Sb flux. The diameters of $GaAs_{1-x}Sb_x$ nanowires with x = 0.18, 0.27, and 0.35 are about 75, 140, and 175 nm, respectively. On the other hand, the lengths of the $GaAs_{1-x}Sb_x$ nanowires are observed to decrease with increasing Sb flux. According to the nanowire growth time used, the axial growth rates of the nanowires can be calculated and they are about 79, 71, and 22 nm/min for the samples with x of 0.18, 0.27 and 0.35, respectively. The possible reasons for the axial and radial growth rates variation of the $GaAs_{1-x}Sb_x$ nanowires are as

DOI: 10.1021/acs.nanolett.6b03326
Nano Lett. 2017, 17, 622–630

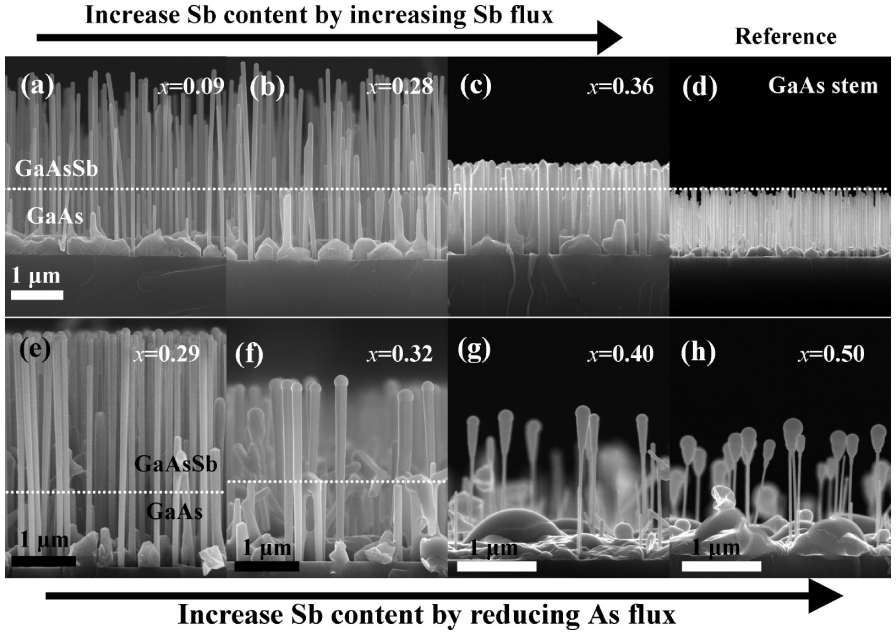

Figure 2. Side-view SEM images of the Ga self-catalyzed GaAs/$GaAs_{1-x}Sb_x$ nanowires grown on Si(111) substrates by MBE. All the GaAs stems have the same growth conditions. (a-c) $GaAs_{1-x}Sb_x$ nanowires were obtained by increasing Sb flux and corresponding x are 0.09, 0.28 and 0.36, respectively. (d) GaAs nanowire stems were shown as a reference. (e–h) $GaAs_{1-x}Sb_x$ nanowires were obtained by reducing As flux and corresponding x are 0.29, 0.32, 0.40, and 0.50, respectively.

follows. It is known that Sb tends to float on top of the growing surface of $GaAs_{1-x}Sb_x$ nanowires due to its surfactant effect. Thus, during nanowire growth Sb and As would exchange at the growing surface[26,36,39−41,46,50] and the surface floating Sb atoms would combine with Ga atoms adsorbed on the (110) nanowire side-facet surfaces, which reduces Ga diffusion on the facets and increases the chance for radial growth.[41] Meanwhile, when a high Sb flux is used, it will hamper Ga diffusion to the catalyst and result in smaller contact angles of the catalyst (it can be observed in our varying Sb flux series), which further causes the droplets to collect less amount of group-V elements and a reduction of the group-V supersaturation. Thus, the hampered Ga side-facets diffusion results in a decrease of the axial growth rate.[50] In our work, the Ga droplets can be clearly distinguished on top of the $GaAs_{1-x}Sb_x$ nanowires with x of 0.18 and 0.27, consistent with growth of these $GaAs_{1-x}Sb_x$ nanowires via a self-catalyzed vapor−liquid−solid mechanism. In contrast, the Ga droplets are almost exhausted for the nanowires with x = 0.35 (Figure 1c). This phenomenon could be attributed to the lack of Ga supplement to support the $GaAs_{1-x}Sb_x$ nanowire growth, especially in the heavy group-V environment, leading to the exhaustion of Ga droplets on the top of nanowires. We attempted to grow $GaAs_{1-x}Sb_x$ nanowires with higher Sb content in this scheme by further increasing the Sb flux, however, it was found that the $GaAs_{1-x}Sb_x$ nanowires become shorter and thicker, and there is almost no nanowire growth on the Si substrates when x > 0.45.

Considering that GaSb nanowire growth needs a relatively low V/III beam equivalent pressure (BEP) ratio of ~2[49] than GaAs nanowire growth of ~7.5, we cannot get higher Sb content $GaAs_{1-x}Sb_x$ nanowires by increasing Sb flux alone as mentioned above. In order to further increase Sb content, we need to increase the Sb/(Sb+As) BEP ratio and reduce the V/III BEP ratio at the same time. To meet these requirements, we grew $GaAs_{1-x}Sb_x$ nanowires on Si substrates by decreasing the As flux. Figure 1d–f shows the side-view SEM images of $GaAs_{1-x}Sb_x$ nanowires grown with As flux of 1.61×10^{-6}, 9.75×10^{-7}, and 4.20×10^{-7} Torr, respectively, and the corresponding x measured by energy-dispersive X-ray spectroscopy (EDX) are 0.30, 0.60, and 0.75. We find that $GaAs_{1-x}Sb_x$ nanowires with x < 0.60 can grow perpendicular to the substrate surface, that is, along the [111] direction. The $GaAs_{1-x}Sb_x$ nanowires with x of 0.30 (Figure 1d) have a high nanowire density and their diameter and axial growth rate are 130 nm and 74 nm/min, respectively. When Sb content increases to 0.60 (Figure 1e), the as-grown wafer has a low nanowire density and the nanowire diameter and axial growth rate are about 192 nm and 49 nm/min, respectively. Further increasing Sb content, the diameter becomes larger and axial growth rate becomes smaller (not shown here). It is also clear that a two-dimensional growth of $GaAs_{1-x}Sb_x$ appears in this sample. Finally, increasing Sb content to 0.75 (Figure 1f) resulted in almost no $GaAs_{1-x}Sb_x$ nanowires and because the two-dimensional growth dominates the $GaAs_{1-x}Sb_x$ growth, a $GaAs_{1-x}Sb_x$ film with a thickness of about 1 μm formed on the substrate surface. $GaAs_{1-x}Sb_x$ nanowires with x = 0.79 were also grown directly on Si(111) substrates in this manner (using a relative low As flux and a high Sb flux). The obtained $GaAs_{1-x}Sb_x$ nanowires have nonuniform diameters and they were enwrapped by the parasitic $GaAs_{1-x}Sb_x$ islands (see Supporting Information Figure S2).

$GaAs_{1-x}Sb_x$ Nanowires Growth on GaAs Nanowire Stems by Tuning the Sb and As Fluxes. The growth of the Ga self-catalyzed GaAs/$GaAs_{1-x}Sb_x$ nanowires with different Sb content was also carried out on Si(111) substrates by MBE, and the Sb content was varied by tuning the Sb and As fluxes. Figure 2a–c shows the side-view SEM images of the $GaAs_{1-x}Sb_x$ nanowires grown with Sb flux of 3.75×10^{-7}, 8.63×10^{-7}, and 1.83×10^{-6} Torr, respectively. We can see from Figure 2a–c that $GaAs_{1-x}Sb_x$ nanowires have been successfully grown on GaAs nanowire stems. The morphologies of $GaAs_{1-x}Sb_x$ nanowires are affected by the Sb flux as observed

DOI: 10.1021/acs.nanolett.6b03326
Nano Lett. 2017, 17, 622−630

in the nanoiwires grown directly on Si(111) substrates. Notably, the $GaAs_{1-x}Sb_x$ nanowire diameter increases with higher Sb flux. The diameters of $GaAs_{1-x}Sb_x$ nanowires with x = 0.09, 0.28, and 0.36 are about 90, 104, and 175 nm, respectively. On the other hand, the lengths of the $GaAs_{1-x}Sb_x$ nanowires are observed to decrease with increasing Sb flux (the axial growth rates are about 49, 46, and 11 nm/min for the samples with x of 0.09, 0.28 and 0.36, respectively). $GaAs_{1-x}Sb_x$ nanowires grown with the Sb flux of 1.83×10^{-6} Torr have a length only about 500 nm with the growth time of 45 min (Figure 2c). Further increasing the Sb flux, no $GaAs_{1-x}Sb_x$ nanowires can be grown on GaAs nanowire stems owing to the exhaustion of Ga droplets on the top of nanowires as discussed above.

$GaAs_{1-x}Sb_x$ nanowires were also grown on GaAs nanowire stems by decreasing the As flux. Figure 2e–h shows the side-view SEM images of the $GaAs_{1-x}Sb_x$ nanowires grown with As flux of 1.61×10^{-6}, 1.35×10^{-6}, 1.05×10^{-6} and 9.75×10^{-7} Torr, respectively, the corresponding x measured by EDX are 0.29, 0.32, 0.40, and 0.50. We find that $GaAs_{1-x}Sb_x$ nanowires with $x \leq 0.50$ can be grown on GaAs nanowire stems. It can be seen that $GaAs_{1-x}Sb_x$ nanowires grown with As flux of 1.61×10^{-6} and 1.35×10^{-6} Torr have a uniform diameter and relative long length. Their diameters are about 121 and 175 nm, respectively. Their lengths are about 2.4 and 1.4 μm, respectively (corresponding axial growth rates: ~ 53 and 30 nm/min). However, further decreasing the As flux to 1.05×10^{-6} and 9.75×10^{-7} Torr, taping morphology $GaAs_{1-x}Sb_x$ nanowires appear and they have a low growth rate (~16 and 10 nm/min, respectively). $GaAs_{1-x}Sb_x$ nanowires grown with low As flux will cause the droplets to collect less amount of group-V elements and a reduction of the group-V supersaturation.[51,52] Thus, the growth rate of $GaAs_{1-x}Sb_x$ nanowires decreases with lower As flux. We attempted to grow $GaAs_{1-x}Sb_x$ nanowires with higher Sb content in this scheme by further decreasing the As flux, however, it was found that the $GaAs_{1-x}Sb_x$ nanowires become shorter and taper, and there is almost no nanowire growth on the GaAs nanowire stems when $x > 0.55$. It is also worth noting that the diameter of GaAs nanowire stem decreases with lower As flux (Figure 2g,h). This phenomenon is caused by the part decomposition of GaAs nanowire stems before and during the growth of $GaAs_{1-x}Sb_x$ segments.

$GaAs_{1-x}Sb_x$ Nanowire Growth on GaAs Nanowire Stems by Tuning the As Backgroud. According to above results, $GaAs_{1-x}Sb_x$ nanowires with low Sb content can be grown directly on Si(111) substrates ($0 \leq x \leq 0.60$) and GaAs nanowire stems ($0 \leq x \leq 0.50$) by tuning the Sb and As fluxes. The former (grown directly on Si substrates) has a relative higher axial growth rate and a relative broader composition range (see Supporting Information Section 1) than the latter (grown on GaAs nanowire stems). Meanwhile, we find that $GaAs_{1-x}Sb_x$ nanowires with $x > 0.60$ and good morphology cannot be obtained by tuning the Sb and As fluxes. On one hand, with increasing the Sb flux, the exhaustion of Ga droplets on the top of $GaAs_{1-x}Sb_x$ nanowires will hinder the axial growth of nanowires (as shown in Figure 1a–c and Figure 2a–c). On the other hand, with decreasing the As flux, although we notice that the Ga droplets can always exist on the top of $GaAs_{1-x}Sb_x$ nanowires, the reduction of the group-V supersaturation will be harmful to the axial growth of nanowires (as shown in Figure 1d–f and Figure 2e–h). We know that the pure GaSb nanowires can be successfully grown on GaAs or InAs nanowire stems using MOCVD and MOVPE,[24,28–35] where there is homogeneous As atmosphere during nanowire growth. Thus, to minimize the possible negative effect from the directional characteristic of the As flux in the MBE chamber[53] and from the Sb content increase on nanowire morphology, we grew the $GaAs_{1-x}Sb_x$ nanowires with higher Sb content by tuning the As background.

Figure 3a–d shows the side-view SEM images of the $GaAs_{1-x}Sb_x$ nanowires grown on GaAs nanowire stems at different As background fluxes, and the corresponding x in the nanowires are 0.54, 0.70, 0.80 and 0.93, respectively (detailed growth conditions are shown in Table S1). Evidently, the $GaAs_{1-x}Sb_x$ nanowires are well grown on the GaAs nanowire stems. All the $GaAs_{1-x}Sb_x$ nanowires have diameters larger than those of the GaAs segments, which is often observed in antimony-based nanowires.[29,54] The diameters of $GaAs_{1-x}Sb_x$ nanowires in Figure 3a–d are about 225, 230, 240, and 285 nm and their axial growth rates are about 26, 19, 16, and 12 nm/min, respectively. The relatively low axial growth rate is caused by the increase of Sb content in the nanowires. It is worth noting that the Ga droplets can be observed clearly on top of the $GaAs_{1-x}Sb_x$ nanowires even when x is as high as 0.93. The existence of Ga droplets is strong evidence for the successful growth of $GaAs_{1-x}Sb_x$ nanowires with such high Sb content on the GaAs nanowire stems. Furthermore, it suggests that long $GaAs_{1-x}Sb_x$ nanowires can be obtained by extending the nanowire growth time. We have also experimented with growing $GaAs_{1-x}Sb_x$ nanowires on GaAs nanowire stems at further decreased As background in the MBE chamber. We find that we can obtain almost pure GaSb nanowires on GaAs nanowire stems (As is present at a small amount of around 4% in the GaSb nanowire body) although they have a very low axial growth rate.[49] To enlarge the Sb composition range, Ga self-catalyzed GaAs/$GaAs_{1-x}Sb_x$ nanowires were grown on Si(111) substrates by further increasing the As background flux. We find that $GaAs_{1-x}Sb_x$ nanowires with x of ~0.40 can be grown on GaAs nanowire stems by tuning the As background. Further increasing the As background flux, GaAs/$GaAs_{1-x}Sb_x$ core–

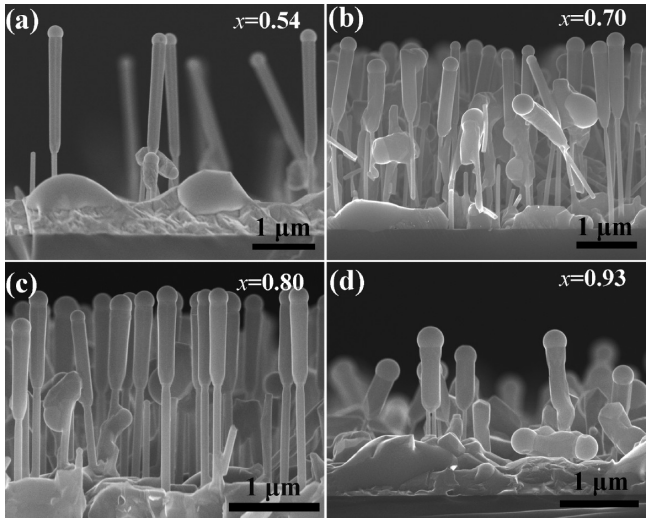

Figure 3. Side-view SEM images of the self-catalyzed $GaAs_{1-x}Sb_x$ nanowires grown on GaAs nanowire stems by MBE. (a–d) $GaAs_{1-x}Sb_x$ nanowires with x of 0.54, 0.70, 0.80, and 0.93 respectively obtained by reducing the As flux, using the As background in the MBE chamber as "As source".

DOI: 10.1021/acs.nanolett.6b03326
Nano Lett. 2017, 17, 622–630

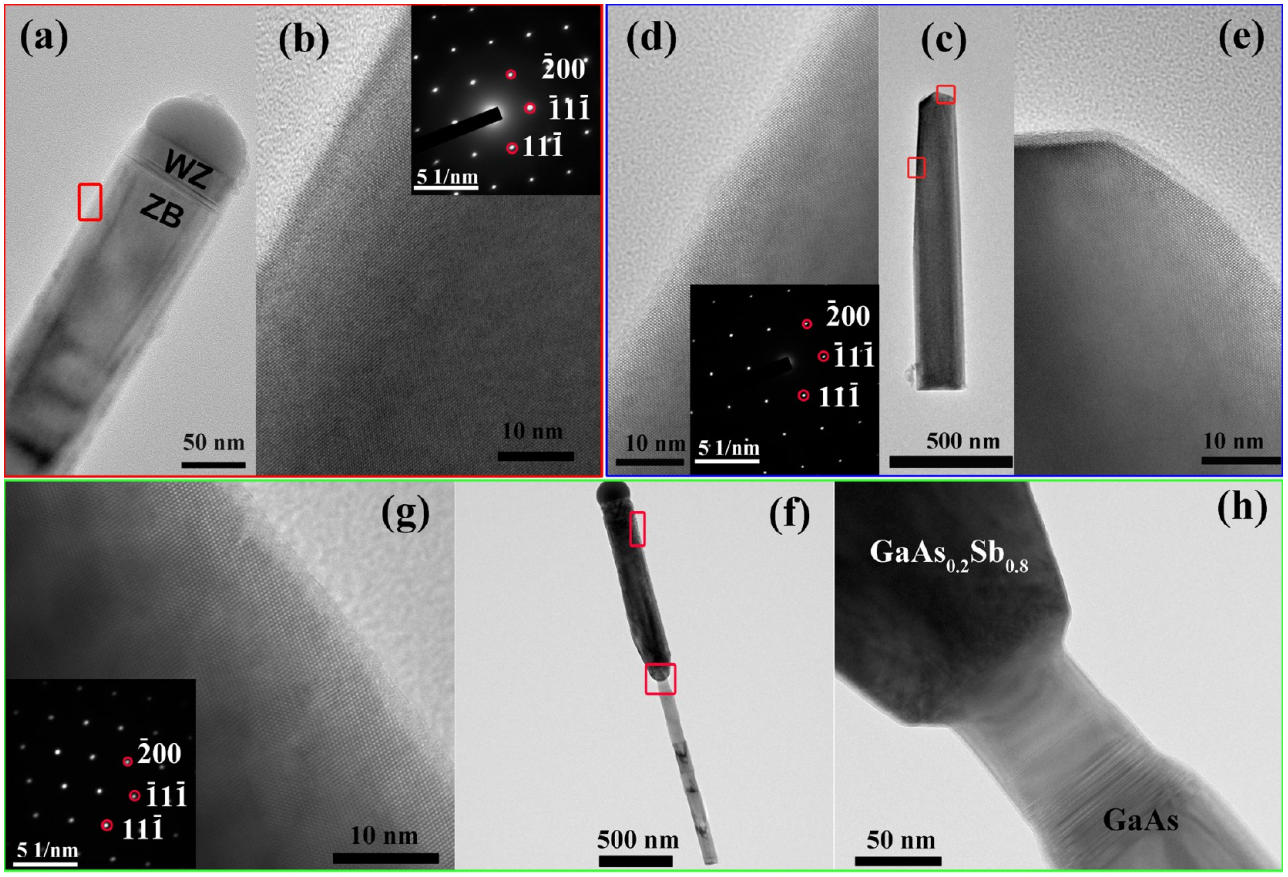

Figure 4. (a,b) TEM images of a $GaAs_{1-x}Sb_x$ nanowire with x of 0.18, (c–e) TEM images of a $GaAs_{1-x}Sb_x$ nanowire with x of 0.35. (g,h) TEM images of a GaAs/$GaAs_{1-x}Sb_x$ heterostructure nanowire with x of 0.80 (f). The insets of (b,d,g) are their corresponding SAED patterns.

shell nanowires formed on Si(111) substrates (see Supporting Information Section 3).

On the basis of the above results, we find that the growth window of the $GaAs_{1-x}Sb_x$ nanowires grown directly on Si(111) substrates and GaAs nanowire stems is strongly dependent on the Sb and As fluxes and the As background. By careful tuning these growth parameters, we can realize the Ga self-catalyzed growth of near full-composition-range energy-gap-tunable $GaAs_{1-x}Sb_x$ nanowires in our MBE system.

Crystal Structure of $GaAs_{1-x}Sb_x$ Nanowires. The crystal structure of the $GaAs_{1-x}Sb_x$ nanowires was investigated by transmission electron microscopy (TEM). Figure 4a,b shows the TEM images of a typical $GaAs_{1-x}Sb_x$ nanowire with x of 0.18 (Figure 1a). The inset of Figure 4b is a selective area electron diffraction pattern (SAED) of the nanowire, which is indexed to the face-centered cubic phase of the $GaAs_{1-x}Sb_x$ viewed along the [011] axis. Detailed high-resolution TEM (HRTEM) and SAED results reveal that the $GaAs_{1-x}Sb_x$ nanowire is of a pure ZB crystal structure, with the exception of a very short wurtzite (WZ) section (~30 nm) at the tip. In our work, at the end of nanowire growth the Sb, As, and Ga source shutters were closed at the same time. Thus, the Ga droplet and As atmosphere in the MBE chamber could exist for a while, while Sb would be exhausted almost immediately because of its small flux in comparison with As. A transition from ZB to WZ/stacking faults appears when the triple phase line passes through the edges between the top and side facets of the nanowires.[41,47,52,55] Here, the influence of a small amount of Sb addition on the crystal structure reported in the literature can be neglected.[41] The very short WZ section is only observed in $GaAs_{1-x}Sb_x$ nanowires with low Sb content in our work. Figure 4c–e shows the TEM images of a typical $GaAs_{1-x}Sb_x$ nanowire with x of 0.35. From Figure 4c, we can see that there is no Ga droplet on top of the $GaAs_{1-x}Sb_x$ nanowire, which is consistent with the SEM results above (Figure 1c). Detailed HRTEM and SAED results indicate that the entire $GaAs_{1-x}Sb_x$ nanowire body has a pure ZB structure. According to the literature, Sb addition will reduce supersaturation of group-V elements in Ga droplet and affect the additional cohesive energy required for the formation of a WZ stacking order.[41] Thus, a pure ZB crystal structure is obtained in the high Sb content $GaAs_{1-x}Sb_x$ nanowires. Improving the nanowire crystalline quality by Sb addition has also been reported in other Sb-based III–V ternary nanowires.[20,50] TEM results also show that $GaAs_{1-x}Sb_x$ nanowires grown on the GaAs nanowire stems have high crystalline quality. Figure 4f–h shows typical TEM images of a GaAs/$GaAs_{1-x}Sb_x$ heterostructure nanowire with x of 0.80 (SEM image in Figure 3c). It is apparent that the entire $GaAs_{1-x}Sb_x$ section has a pure ZB crystal structure. The detailed crystal structure and chemical composition information on the GaAs/$GaAs_{1-x}Sb_x$ heterostructure nanowires with different Sb content are given in Supporting Information Section 4.

Photoluminescence Spectra of $GaAs_{1-x}Sb_x$ Nanowires. The optical properties of the $GaAs_{1-x}Sb_x$ nanowires grown above were studied by μ-PL spectra at 77 K. Here, the GaAs nanowires were used as a reference sample. Figure 5a shows the representative PL spectra of the Ga self-catalyzed

DOI: 10.1021/acs.nanolett.6b03326
Nano Lett. 2017, 17, 622–630

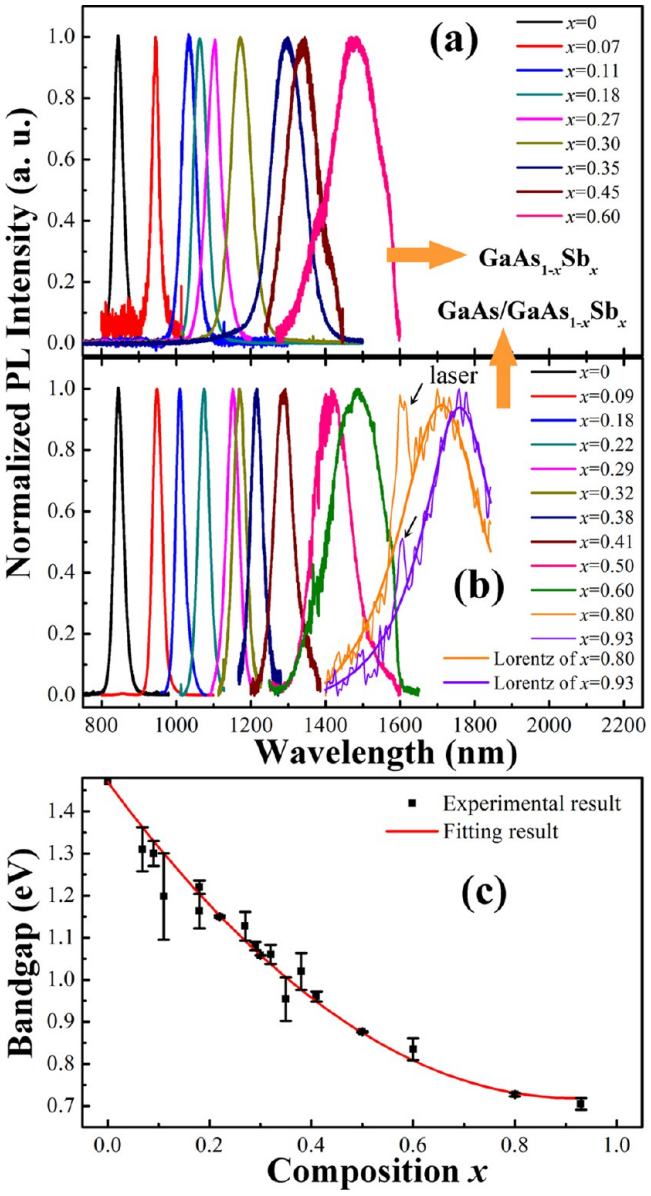

Figure 5. (a) The normalized PL spectra of $GaAs_{1-x}Sb_x$ nanowires with different Sb content grown directly on Si(111) substrates at 77 K. (b) The normalized PL spectra of $GaAs_{1-x}Sb_x$ nanowires with different Sb content grown on GaAs nanowire stems at 77 K (c) The resulting bandgap energy of $GaAs_{1-x}Sb_x$ nanowires as a function of Sb composition x. The red curve in (c) is the best fit to the experimental data using a quadratic function.

$GaAs_{1-x}Sb_x$ nanowires grown directly on Si(111) substrates. As shown in Figure 5a, with increasing x from 0 to 0.60 the PL peak of the $GaAs_{1-x}Sb_x$ nanowires can be tuned from 844 nm (1.47 eV, GaAs nanowires) to 1480 nm (0.84 eV, $GaAs_{0.4}Sb_{0.6}$ nanowires). The obtained band-edge emission peaks are consistent with the results reported in $GaAs_{1-x}Sb_x$ nanowires with low Sb compositions.[38,41,45] Figure 5b shows the representative PL spectra of the self-catalyzed $GaAs_{1-x}Sb_x$ nanowires grown on GaAs nanowire stems. As shown in Figure 5b, with increasing x from 0 to 0.93, the PL peak of the $GaAs_{1-x}Sb_x$ nanowires can be tuned from 844 nm (1.47 eV, GaAs nanowires) to 1760 nm (0.71 eV, $GaAs_{0.07}Sb_{0.93}$ nanowires), covering a broad region of the near-infrared spectrum (the PL spectra of $GaAs_{1-x}Sb_x$ nanowires with x of 0.80 and 0.93 are shown in Supporting Information, Figure S7). The bandgap of the $GaAs_{1-x}Sb_x$ nanowires is tuned by 0.76 eV. We note that the PL spectra taken from $GaAs_{1-x}Sb_x$ nanowires of different Sb content show no midgap emission band, indicating that the $GaAs_{1-x}Sb_x$ nanowires have high crystalline quality. This is consistent with the TEM results (Figure 4, Figure S4, and Figure S5 in Supporting Information). It is worth nothing that the line widths of the band-edge emission peaks of $GaAs_{1-x}Sb_x$ nanowires with the above two growth modes consecutively increase with increasing Sb content. The increased alloy broadening with higher Sb content in the $GaAs_{1-x}Sb_x$ nanowires is the possible reason for this phenomenon[56−58] and similar phenomenon has been observed in $GaAs_{1-x}Sb_x$ nanowires,[41] $GaAs/GaAs_{1-x}Sb_x$ core−shell nanowires[48] and $InAs_{1-x}Sb_x$ nanowires.[59] Besides, for the PL spectra of $GaAs_{1-x}Sb_x$ nanowires with high Sb content we can observe that their intensities appear to be weaker than those of the low Sb content nanowires. One of the possible reasons is that a large of surface states exist on the surface of our unpassivated $GaAs_{1-x}Sb_x$ nanowires, which act as nonradiative carrier traps and as a source of potential fluctuations associated with surface-trapped charges;[60−62] With the increase of Sb content, the hole concentration in $GaAs_{1-x}Sb_x$ nanowires increases, which results in the increase of surface recombination velocity in $GaAs_{1-x}Sb_x$ nanowires.[63] Thus, high surface recombination velocities and nonradiative recombination due to surface states strongly degrade the internal quantum efficiency of the high Sb content $GaAs_{1-x}Sb_x$ nanowires.[62]

Although $GaAs_{1-x}Sb_x$ nanowires were grown by two different modes, they followed the same rule of band-edge emission. We also investigated the relationship between the Sb concentration and bandgap energy of the $GaAs_{1-x}Sb_x$ nanowires. From the 77 K PL spectra (Figure 5a,b), we obtained the bandgap energies of the $GaAs_{1-x}Sb_x$ nanowires, and we used EDX to determine the Sb concentration. The black squares in Figure 5c represent the resulting bandgap energy of the $GaAs_{1-x}Sb_x$ nanowires with different Sb content at 77 K. It is known that the bandgap of a ternary alloy is largely determined by an interpolation between those of the two binaries, and we obtained a best fit to the experimental results of the bandgap as a function of composition using a quadratic eq (eq 1, C, a, b, c are fitting parameters).[64] The fitting is constrained by the bandgap of GaAs at x = 0. The red curve in Figure 5c shows the fitting result. The fitting parameters a, b, and c are 1.470, −1.638, and 0.893, respectively. We can use fitting function to calculate the bandgap of the GaSb nanowires at 77 K, and the calculated value is 0.725 eV, ~75 meV smaller than the theoretical value for GaSb films at 77 K (0.8 eV).

$$E_g(GaAs_{(1-x)}Sb_x) = xE_g(GaSb) + (1-x)E_g(GaAs) - Cx(1-x) = a + bx + cx^2 \quad (1)$$

Raman Spectra of $GaAs_{1-x}Sb_x$ Nanowires. Micro-Raman spectroscopy measurements were performed on $GaAs_{1-x}Sb_x$ nanowires with x varying from 0 to 0.93 at room temperature. The spot size of the laser beam used for the Raman measurements is about 1 μm, so it can be focused on a very small region with very few nanowires (1−3). Figure 6a shows the Raman spectra of $GaAs_{1-x}Sb_x$ nanowires with x ranging from 0 to 0.93. We used bulk GaSb and GaAs nanowires as reference samples. The Raman spectrum of GaSb has two peaks at around 226.7 and 235.5 cm^{-1}, which correspond to the transverse optical (TO) and longitudinal

DOI: 10.1021/acs.nanolett.6b03326
Nano Lett. 2017, 17, 622−630

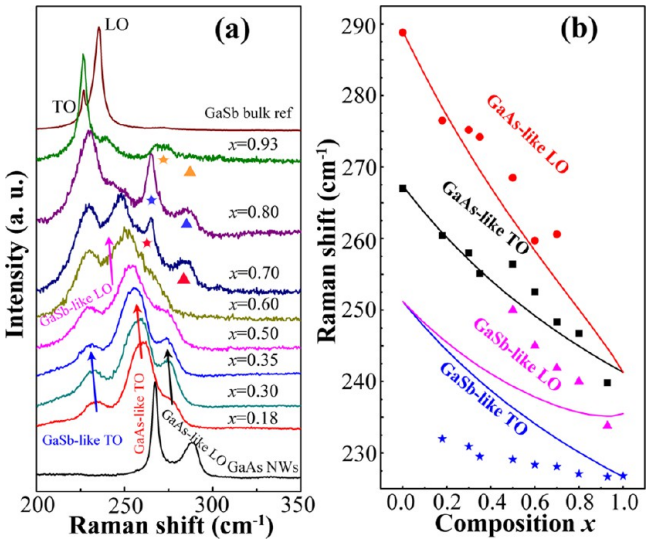

Figure 6. (a) Confocal Raman spectra of $GaAs_{1-x}Sb_x$ nanowires with different Sb content at room temperature. The GaSb-like TO and LO, and GaAs-like TO and LO modes are present in the spectra, the Sb content increases followed by redshift of the four modes. And for $GaAs_{1-x}Sb_x$ nanowires grown on GaAs stems the GaAs TO and LO modes from GaAs stems also appear marked with asterisk and triangle. (b) Phonon mode frequencies of the alloy nanowires as a function of Sb composition x are shown (scatter). Experimental Raman frequencies are obtained from fitting the spectra to Lorentzian functions. Calculated results correspond to the expected frequency are shown by solid lines.

optical (LO) phonon modes of bulk GaSb, respectively.[65] For GaAs nanowires, the TO and LO modes are located at around 267.4 and 289 cm^{-1} respectively.[66] In Figure 6a, two sets of TO and LO phonons are observed for the $GaAs_{1-x}Sb_x$ nanowires and can be assigned as GaAs-like and GaSb-like respectively, whose frequencies varying continuously with Sb content from those for the pristine GaAs and GaSb, respectively.[38,40] This is known as two-mode behaviors of optical phonons in semiconductor alloys. The two-mode behavior has been observed for most of III−V alloys, such as GaAsSb, GaInAs, and GaAsP.[67−69] It indicates that the doping of Sb in GaAs introduces the microscope strain effects and high degree of disorders, which can be confirmed by the broader peaks compared with the corresponding modes in intrinsic GaAs and GaSb. The Raman spectra were fitted with Lorentzian lineshapes to obtain the observed peak frequencies (see Supporting Information Figure S8). For GaAs/$GaAs_{1-x}Sb_x$ nanowires, GaAs-like LO and TO peaks from GaAs nanowire stems are also observed which marked with asterisk and triangle.

The observed peak frequencies are depicted in Figure 6b as a function of the Sb compositions. As the Sb content is increased, GaAs-like TO and LO phonons in $GaAs_{1-x}Sb_x$ nanowires shift to lower frequencies with increasing Sb content in comparison with that for intrinsic vibrational modes of pure GaAs nanowires. Because Sb is a heavier atom than As, and the increase of Sb atomic concentration in the $GaAs_{1-x}Sb_x$ nanowires is expected to decrease the phonon frequencies.[14,70]

For the same reason, GaSb-like TO and LO shift to low frequencies with the increase of Sb content. The redshift of GaAs- and GaSb-like TO and LO appear more clearly with the Sb content ranging from 0 to 0.93. It is worth noting that GaSb-like TO and GaAs-like TO can be detected over the whole Sb compositional range in $GaAs_{1-x}Sb_x$ nanowires (0−0.93), while GaSb-like LO (GaAs-like LO) was not detected in low (high) Sb content. This is expected, because the intensity of the LO mode in nanowires is much lower than that of the TO mode,[38] the GaSb-like LO (GaAs-like LO) being not very intense due to the relatively low (high) concentration in Sb. The detailed analysis of the frequencies shifts for Raman modes by theory calculation is shown in Supporting Information Section 6.

Electronic Properties of $GaAs_{1-x}Sb_x$ Nanowires. We characterized the electrical properties of individual $GaAs_{1-x}Sb_x$ nanowires with different Sb content using a two-terminal device geometry (a typical SEM image of single $GaAs_{1-x}Sb_x$ nanowire back-gated FET device is shown in the inset in Figure 7d) with

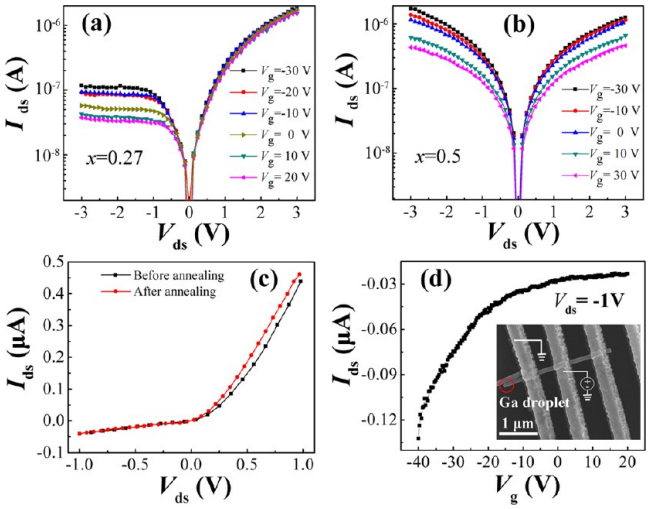

Figure 7. (a) Rectifying behavior in a $GaAs_{1-x}Sb_x$ (x = 0.27) nanowire FET device, while disappears in the higher Sb content (x = 0.50) device (b). (c) Comparison of the $I-V$ characteristics of a $GaAs_{1-x}Sb_x$ nanowire device before and after RTA process. (d) Transfer characteristics of a nanowire device with x = 0.27, indicating a p-type characteristic. Inset in (d) shows typical SEM image of a single $GaAs_{1-x}Sb_x$ nanowire device and the red circle marks the Ga droplet.

the bias applied to the drain electrode and the source electrode grounded. Figure 7a shows the typical semilog current−voltage ($I-V$) characteristics of a $GaAs_{1-x}Sb_x$ nanowire device with x = 0.27. From Figure 7a, a rectifying behavior is clearly observed. The direction of the current rectification is the same in all studied low Sb content nanowires which is determined by the nanowire growth direction.[40] The current rectification ratio ($I_{forward}/I_{reverse}$) is about 10 at a voltage range of ±1 V. However, when we increase x to 0.50 and above, the rectifying behavior of the $GaAs_{1-x}Sb_x$ nanowire device disappears (see Supporting Information Figure S9). The field-effect measurements show that holes are the majority carrier in the $GaAs_{1-x}Sb_x$ nanowires, as shown in Figure 7a−b. To investigate the rectifying behavior, we have subject the nanowire device with x = 0.27 to rapid thermal annealing (RTA) under N_2 ambience at 430 °C for 30 s. Comparing the $I-V$ curves from the nanowire device before and after RTA, we find that the rectifying behavior persists after such a process, as shown in Figure 7c. Figure 7d shows the transfer characteristics at V_{ds} = −1 V of the $GaAs_{1-x}Sb_x$ nanowire device with x = 0.27, which confirms that holes are the majority carrier, and the gate modulation effect is comparable to that observed in Huh et al.'s work. Huh et al.[40] reported that the rectifying behavior observed in

DOI: 10.1021/acs.nanolett.6b03326
Nano Lett. 2017, 17, 622−630

$GaAs_{1-x}Sb_x$ nanowire devices could be attributed to asymmetric Schottky contacts which formed between the nanowire and the metal electrodes near the base and the top of the nanowire and caused by gradual distribution of carrier and Sb concentration. In our work, the rectifying behavior in low Sb content $GaAs_{1-x}Sb_x$ nanowire devices might be caused by the same reason, although the variation of Sb composition in single $GaAs_{1-x}Sb_x$ nanowire is much less than the result in ref 40. With the increase of Sb content, the carrier concentration in the $GaAs_{1-x}Sb_x$ nanowire increase,[71] which could reduce Schottky contacts barrier and Ohmic contact tends to form between the nanowire and the metal electrodes as we observed in Figure 7b and Figure S9b–d.

In conclusion, Ga self-catalyzed $GaAs_{1-x}Sb_x$ nanowires have been systematically grown by MBE and their structure and optoelectronic properties were carefully characterized. $GaAs_{1-x}Sb_x$ nanowires can be grown directly on Si(111) substrates ($0 \le x \le 0.60$) and GaAs nanowire stems ($0 \le x \le 0.50$) by tuning the Sb and As fluxes. To obtain $GaAs_{1-x}Sb_x$ nanowires with a large range of tunable bandgaps, we grow them on GaAs nanowire stems by tuning the As background in which Sb content reaches up to 0.93. PL analysis confirms that the emission wavelength of the $GaAs_{1-x}Sb_x$ nanowires is tuned from 844 nm (GaAs) to 1760 nm ($GaAs_{0.07}Sb_{0.93}$). The $GaAs_{1-x}Sb_x$ nanowires have pure ZB structure. The optical phonons of the $GaAs_{1-x}Sb_x$ nanowires show redshift with x increasing from 0 to 0.93. Rectifying behavior is observed in FET devices based on individual $GaAs_{1-x}Sb_x$ nanowires with low Sb content, wherreas for high Sb content nanowires, Ohmic contact tends to form between the nanowire and the metal electrodes and the rectifying behavior disappears. The successful growth of high-quality $GaAs_{1-x}Sb_x$ nanowires with large-range bandgap tuning provides ample opportunities for advanced device engineering of near-IR detectors and sources.

■ ASSOCIATED CONTENT

Supporting Information

The Supporting Information is available free of charge on the ACS Publications website at DOI: 10.1021/acs.nanolett.6b03326.

Detailed growth procedures, growth parameters and equipment for $GaAs_{1-x}Sb_x$ and $GaAs/GaAs_{1-x}Sb_x$ nanowire growth and characterization; SEM images of $GaAs_{1-x}Sb_x$ nanowires grown directly on Si(111) substrates; SEM images of $GaAs_{1-x}Sb_x$ nanowires grown on GaAs nanowire stems by increasing the As background flux; structure and composition information on $GaAs/GaAs_{1-x}Sb_x$ nanowires; full PL spectra of $GaAs_{1-x}Sb_x$ nanowire with x of 0.80 and 0.93; fitting the Raman spectra with Lorentzian lineshapes and detailed analysis of the frequencies shifts for Raman modes; electrical properties of FET devices based on $GaAs_{1-x}Sb_x$ nanowires of different Sb content (PDF)

■ AUTHOR INFORMATION

Corresponding Authors

*E-mail: pandong@semi.ac.cn.
*E-mail: jhzhao@red.semi.ac.cn.

ORCID

Anlian Pan: 0000-0003-3335-3067
Jianhua Zhao: 0000-0003-2269-3963

Notes

The authors declare no competing financial interest.

■ ACKNOWLEDGMENTS

The authors acknowledge Peng Xiong at Florida State University for discussion. This work was supported by the MOST of China (Nos. 2013CB922303, 2015CB921503, and 2016YFA0301200) and NSF of China (Nos. 61334006, 61504133, 61404127, 11225421, 11434010, and 11474277). D. P. and X. Y. also acknowledge the support from Youth Innovation Promotion Association, CAS.

■ REFERENCES

(1) Pan, C. H.; Lee, C. P. *J. Appl. Phys.* **2013**, *113*, 043112.
(2) Hu, J.; Xu, X. G.; Stotz, J. A. H.; Watkins, S. P. A.; Curzon, E. M. L.; Thewalt, W.; Matine, N. *Appl. Phys. Lett.* **1998**, *73*, 2799.
(3) Miura, K.; Iguchi, Y.; Tsubokura, M.; Kawamura, Y. *J. Appl. Phys.* **2013**, *113*, 143506.
(4) Dowd, P.; Johnson, S. R.; Feld, S. A.; Adamcyk, M.; Chaparro, S. A.; Joseph, J.; Hilgers, K.; Horning, M. P.; Shiralagi, K.; Zhang, Y. H. *Electron. Lett.* **2003**, *39*, 987.
(5) Bajo, M. M.; Ulloa, J. M.; del Moral, M.; Guzmán, Á.; Hierro, A. *IEEE J. Quantum Electron.* **2011**, *47*, 1547.
(6) Blume, G.; Hild, K.; Marko, I. P.; Hosea, T. J. C.; Yu, S. Q.; Chaparro, S. A.; Samal, N.; Johnson, S. R.; Zhang, Y. H.; Sweeney, S. J. *J. Appl. Phys.* **2012**, *112*, 033108.
(7) Sun, X. G.; Wang, S. L.; Hsu, J. S.; Sidhu, R.; Zheng, X. G.; Li, X. W.; Campbell, J. C.; Holmes, A. L., Jr. *IEEE J. Sel. Top. Quantum Electron.* **2002**, *8*, 817.
(8) Hossain, N.; Hild, K.; Jin, S. R.; Yu, S. Q.; Johnson, S. R.; Ding, D.; Zhang, Y. H.; Sweeney, S. J. *Appl. Phys. Lett.* **2013**, *102*, 041106.
(9) Dvorak, M. W.; Bolognesi, C. R.; Pitts, O. J.; Watkins, S. P. *IEEE Electron Device Lett.* **2001**, *22*, 361.
(10) Qiu, W. Y.; Wang, X. J.; Chen, P. P.; Li, N.; Lu, W. *Appl. Phys. Lett.* **2014**, *105*, 082104.
(11) Hall, K. C.; Leonard, S. W.; van Driel, H. M.; Kost, A. R.; Selvig, E.; Chow, D. H. *Appl. Phys. Lett.* **1999**, *75*, 3665.
(12) Qiu, W. Y.; Zhang, B.; Wang, Y. F.; Chen, P. P.; Chen, Z. H.; Li, N.; Lu, W.; Wang, X. J. *Appl. Phys. Express* **2016**, *9*, 021201.
(13) Chou, L. C.; Lin, Y. R.; Wan, C. T.; Lin, H. H. *Microelectron. J.* **2006**, *37*, 1511.
(14) Chen, Y. R.; Chou, L. C.; Yang, Y. J.; Lin, H. H. *J. Phys. D: Appl. Phys.* **2013**, *46*, 035306.
(15) Liang, Y.; Nix, W. D.; Griffin, P. B.; Plummer, J. D. *J. Appl. Phys.* **2005**, *97*, 043519.
(16) Glas, F. *Phys. Rev. B: Condens. Matter Mater. Phys.* **2006**, *74*, 121302.
(17) Duan, X. F.; Lieber, C. M. *Adv. Mater.* **2000**, *12*, 298.
(18) Ganjipour, B.; Ek, M.; Borg, B. M.; Dick, K. A.; Pistol, M.-E.; Wernersson, L.-E.; Thelander, C. *Appl. Phys. Lett.* **2012**, *101*, 103501.
(19) Xu, T.; Dick, K. A.; Plissard, S.; Nguyen, T. H.; Makoudi, Y.; Berthe, M.; Nys, J.-P.; Wallart, X.; Grandidier, B.; Caroff, P. *Nanotechnology* **2012**, *23*, 095702.
(20) Sourribes, M. J. L.; Isakov, I.; Panfilova, M.; Liu, H. Y.; Warburton, P. A. *Nano Lett.* **2014**, *14*, 1643.
(21) Zhou, H. L.; Pozuelo, M.; Hicks, R. F.; Kodambaka, S. *J. Cryst. Growth* **2011**, *319*, 25.
(22) Ghalamestani, S. G.; Ek, M.; Ganjipour, B.; Thelander, C.; Johansson, J.; Caroff, P.; Dick, K. A. *Nano Lett.* **2012**, *12*, 4914.
(23) Ma, L.; Hu, W.; Zhang, Q. L.; Ren, P. Y.; Zhuang, X. J.; Zhou, H.; Xu, J. Y.; Li, H. L.; Shan, Z. P.; Wang, X. X.; Liao, L.; Xu, H. Q.; Pan, A. L. *Nano Lett.* **2014**, *14*, 694.
(24) Guo, Y. N.; Zou, J.; Paladugu, M.; Wang, H.; Gao, Q.; Tan, H. H.; Jagadish, C. *Appl. Phys. Lett.* **2006**, *89*, 231917.
(25) Tchernycheva, M.; Cirlin, G. E.; Patriarche, G.; Travers, L.; Zwiller, V.; Perinetti, U.; Harmand, J. C. *Nano Lett.* **2007**, *7*, 1500.
(26) Yuan, X. M.; Caroff, P.; Wong-Leung, J.; Tan, H. H.; Jagadish, C. *Nanoscale* **2015**, *7*, 4995.

DOI: 10.1021/acs.nanolett.6b03326
Nano Lett. 2017, 17, 622–630

(27) Li, Z. Y.; Yuan, X. M.; Fu, L.; Peng, K.; Wang, F.; Fu, X.; Caroff, P.; White, T. P.; Tan, H. H.; Jagadish, C. *Nanotechnology* **2015**, *26*, 445202.
(28) Jeppsson, M.; Dick, K. A.; Nilsson, H. A.; Sköld, N.; Wagner, J. B.; Caroff, P.; Wernersson, L.-E. *J. Cryst. Growth* **2008**, *310*, 5119.
(29) Jeppsson, M.; Dick, K. A.; Wagner, J. B.; Caroff, P.; Deppert, K.; Samuelson, L.; Wernersson, L.-E. *J. Cryst. Growth* **2008**, *310*, 4115.
(30) Ganjipour, B.; Nilsson, H. A.; Mattias Borg, B.; Wernersson, L.-E.; Samuelson, L.; Xu, H. Q.; Thelander, C. *Appl. Phys. Lett.* **2011**, *99*, 262104.
(31) Ganjipour, B.; Dey, A. W.; Borg, B. M.; Ek, M.; Pistol, M. E.; Dick, K. A.; Wernersson, L. E.; Thelander, C. *Nano Lett.* **2011**, *11*, 4222.
(32) Borg, B. M.; Dick, K. A.; Ganjipour, B.; Pistol, M. E.; Wernersson, L. E.; Thelander, C. *Nano Lett.* **2010**, *10*, 4080.
(33) Ek, M.; Borg, B. M.; Dey, A. W.; Ganjipour, B.; Thelander, C.; Wernersson, L.-E.; Dick, K. A. *Cryst. Growth Des.* **2011**, *11*, 4588.
(34) Ek, M.; Borg, B. M.; Johansson, J.; Dick, K. A. *ACS Nano* **2013**, *7*, 3668.
(35) de la Mata, M.; Magen, C.; Caroff, P.; Arbiol, J. *Nano Lett.* **2014**, *14*, 6614.
(36) Yang, Z. X.; Han, N.; Fang, M.; Lin, H.; Cheung, H. Y.; Yip, S. P.; Wang, E. J.; Hung, T.; Wong, C. Y.; Ho, J. C. *Nat. Commun.* **2014**, *5*, 5249.
(37) Ma, L.; Zhang, X. H.; Li, H. L.; Tan, H.; Yang, Y. K.; Xu, Y. D.; Hu, W.; Zhu, X. L.; Zhuang, X. J.; Pan, A. L. *Semicond. Sci. Technol.* **2015**, *30*, 105033.
(38) Alarcón-Lladó, E.; Conesa-Boj, S.; Wallart, X.; Caroff, P.; Fontcuberta i Morral, A. *Nanotechnology* **2013**, *24*, 405707.
(39) Conesa-Boj, S.; Kriegner, D.; Han, X.; Plissard, S.; Wallart, X.; Stangl, J.; Fontcuberta i Morral, A.; Caroff, P. *Nano Lett.* **2014**, *14*, 326.
(40) Huh, J.; Yun, H.; Kim, D. C.; Munshi, A. M.; Dheeraj, D. L.; Kauko, H.; van Helvoort, A. T. J.; Lee, S.; Fimland, B.-O.; Weman, H. *Nano Lett.* **2015**, *15*, 3709.
(41) Ren, D. D.; Dheeraj, D. L.; Jin, C. J.; Nilsen, J. S.; Huh, J.; Reinertsen, J. F.; Munshi, A. M.; Gustafsson, A.; van Helvoort, A. T. J.; Weman, H.; Fimland, B. O. *Nano Lett.* **2016**, *16*, 1201.
(42) Dheeraj, D. L.; Patriarche, G.; Zhou, H.; Harmand, J. C.; Weman, H.; Fimland, B. O. *J. Cryst. Growth* **2009**, *311*, 1847.
(43) Dheeraj, D. L.; Patriarche, G.; Zhou, H.; Hoang, T. B.; Moses, A. F.; Grønsberg, S.; van Helvoort, A. T.; Fimland, B.-O.; Weman, H. *Nano Lett.* **2008**, *8*, 4459.
(44) Plissard, S.; Dick, K. A.; Wallart, X.; Caroff, P. *Appl. Phys. Lett.* **2010**, *96*, 121901.
(45) Todorovic, J.; Kauko, H.; Ahtapodov, L.; Moses, A. F.; Olk, P.; Dheeraj, D. L.; Fimland, B. O.; Weman, H.; van Helvoort, A. T. J. *Semicond. Sci. Technol.* **2013**, *28*, 115004.
(46) Kauko, H.; Fimland, B. O.; Grieb, T.; Munshi, A. M.; Müller, K.; Rosenauer, A.; van Helvoort, A. T. J. *J. Appl. Phys.* **2014**, *116*, 144303.
(47) Munshi, A. M.; Dheeraj, D. L.; Todorovic, J.; van Helvoort, A. T. J.; Weman, H.; Fimland, B. O. *J. Cryst. Growth* **2013**, *372*, 163.
(48) Kasanaboina, P. K.; Ojha, S. K.; Sami, S. U.; Reynolds, C. L., Jr; Liu, Y.; Iyer, S. *Semicond. Sci. Technol.* **2015**, *30*, 105036.
(49) Yu, X. Z.; Li, L. X.; Wang, H. L.; Xiao, J. X.; Shen, C.; Pan, D.; Zhao, J. H. *Nanoscale* **2016**, *8*, 10615.
(50) Potts, H.; Friedl, M.; Amaduzzi, F.; Tang, K. C.; Tütüncüoglu, G.; Matteini, F.; Lladó, E. A.; McIntyre, P. C.; Fontcuberta i Morral, A. *Nano Lett.* **2016**, *16*, 637.
(51) Ramdani, M. R.; Gil, E.; Leroux, C.; Andre, Y.; Trassoudaine, A.; Castelluci, D.; Bideux, L.; Monier, G.; Robert-Goumet, C.; Kupka, R. *Nano Lett.* **2010**, *10*, 1836.
(52) Yu, X. Z.; Wang, H. L.; Lu, J.; Zhao, J. H.; Misuraca, J.; Xiong, P.; von Molnar, S. *Nano Lett.* **2012**, *12*, 5436.
(53) Glas, F. *Phys. Status Solidi B* **2010**, *247*, 254.
(54) Pan, D.; Fan, D. X.; Kang, N.; Zhi, J. H.; Yu, X. Z.; Xu, H. Q.; Zhao, J. H. *Nano Lett.* **2016**, *16*, 834.
(55) Krogstrup, P.; Curiotto, S.; Johnson, E.; Aagesen, M.; Nygård, J.; Chatain, D. *Phys. Rev. Lett.* **2011**, *106*, 125505.
(56) Ra, Y. H.; Navamathavan, R.; Park, J. H.; Lee, C. R. *Nano Lett.* **2013**, *13*, 3506.
(57) Zhuang, X. J.; Ning, C. Z.; Pan, A. L. *Adv. Mater.* **2012**, *24*, 13.
(58) Ren, P. Y.; Hu, W.; Zhang, Q. L.; Zhu, X. L.; Zhuang, X. J.; Ma, L.; Fan, X. P.; Zhou, H.; Liao, L.; Duan, X. F.; Pan, A. L. *Adv. Mater.* **2014**, *26*, 7444.
(59) Farrell, A. C.; Lee, W.-J.; Senanayake, P.; Haddad, M. A.; Prikhodko, S. V.; Huffaker, D. L. *Nano Lett.* **2015**, *15*, 6614.
(60) Titova, L. V.; Hoang, T. B.; Jackson, H. E.; Smith, L. M.; Yarrison-Rice, J. M.; Kim, Y.; Joyce, H. J.; Tan, H. H.; Jagadish, C. *Appl. Phys. Lett.* **2006**, *89*, 173126.
(61) Bryant, G. W.; Jaskolski, W. *J. Phys. Chem. B* **2005**, *109*, 19650.
(62) Treu, J.; Stettner, T.; Watzinger, M.; Morkotter, S.; Doblinger, M.; Matich, S.; Saller, K.; Bichler, M.; Abstreiter, G.; Finley, J. J.; Stangl, J.; Koblmuller, G. *Nano Lett.* **2015**, *15*, 3533.
(63) Jastrzebski, L.; Lagowski, J.; Gatos, H. C. *Appl. Phys. Lett.* **1975**, *27*, 537.
(64) Pan, A. L.; Zhou, W. C.; Leong, E. S.; Liu, R. B.; Chin, A. H.; Zou, B. S.; Ning, C. Z. *Nano Lett.* **2009**, *9*, 784.
(65) Liu, F. M.; Zhang, L. D. *J. Cryst. Growth* **1999**, *204*, 19.
(66) Spirkoska, D.; Arbiol, J.; Gustafsson, A.; Conesa-Boj, S.; Glas, F.; Zardo, I.; Heigoldt, M.; Gass, M. H.; Bleloch, A. L.; Estrade, S.; Kaniber, M.; Rossler, J.; Peiro, F.; Morante, J. R.; Abstreiter, G.; Samuelson, L.; Fontcuberta i Morral, A. *Phys. Rev. B: Condens. Matter Mater. Phys.* **2009**, *80*, 245325.
(67) McGlinn, T. C.; Krabach, T. N.; Klein, M. V.; Bajor, G.; Greene, J. E.; Kramer, B.; Barnett, S. A.; Lastras, A.; Gorbatkin, S. *Phys. Rev. B: Condens. Matter Mater. Phys.* **1986**, *33*, 8396.
(68) Groenen, J.; Carles, R.; Landa, G.; Guerret-Piécourt, C.; Fontaine, C.; Gendry, M. *Phys. Rev. B: Condens. Matter Mater. Phys.* **1998**, *58*, 10452.
(69) Pagès, O.; Souhabi, J.; Postnikov, A. V.; Chafi, A. *Phys. Rev. B: Condens. Matter Mater. Phys.* **2009**, *80*, 035204.
(70) Ramkumar, C.; Jain, K.; Abbi, S. *Phys. Rev. B: Condens. Matter Mater. Phys.* **1996**, *53*, 13672.
(71) Hakala, M.; Puska, M. J.; Nieminen, R. M. *J. Appl. Phys.* **2002**, *91*, 4988.

DOI: 10.1021/acs.nanolett.6b03326
Nano Lett. 2017, 17, 622−630